ACCOUNTS
of chemical research

Nanoscaling Laws of Magnetic Nanoparticles and Their Applicabilities in Biomedical Sciences

YOUNG-WOOK JUN, JUNG-WOOK SEO, AND JINWOO CHEON*

Department of Chemistry, Yonsei University, Seoul 120-749, Korea

RECEIVED ON MAY 16, 2007

CONSPECTUS

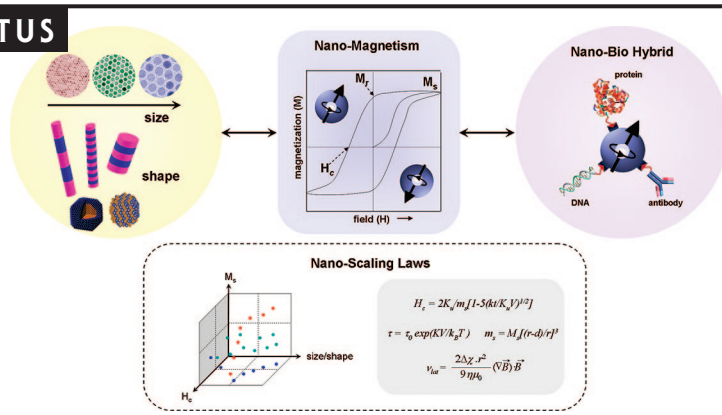

Magnetic nanoparticles, which exhibit a variety of unique magnetic phenomena that are drastically different from those of their bulk counterparts, are garnering significant interest since these properties can be advantageous for utilization in a variety of applications ranging from storage media for magnetic memory devices to probes and vectors in the biomedical sciences. In this Account, we discuss the nanoscaling laws of magnetic nanoparticles including metals, metal ferrites, and metal alloys, while focusing on their size, shape, and composition effects. Their fundamental magnetic properties such as blocking temperature (T_b), spin life time (τ), coercivity (H_c), and susceptibility (χ) are strongly influenced by the nanoscaling laws, and as a result, these scaling relationships can be leveraged to control magnetism from the ferromagnetic to the superparamagnetic regimes. At the same time, they can be used in order to tune magnetic values including H_c, χ, and remanence (M_r). For example, life time of magnetic spin is directly related to the magnetic anisotropy energy (K_uV) and also the size and volume of nanoparticles. The blocking temperature (T_b) changes from room temperature to 10 K as the size of cobalt nanoparticles is reduced from 13 to 2 nm. Similarly, H_c is highly susceptible to the anisotropy of nanoparticles, while saturation magnetization is directly related to the canting effects of the disordered surface magnetic spins and follows a linear relationship upon plotting of $m_s^{1/3}$ vs r^{-1}. Therefore, the nanoscaling laws of magnetic nanoparticles are important not only for understanding the behavior of existing materials but also for developing novel nanomaterials with superior properties.

Since magnetic nanoparticles can be easily conjugated with biologically important constituents such as DNA, peptides, and antibodies, it is possible to construct versatile nano–bio hybrid particles, which simultaneously possess magnetic and biological functions for biomedical diagnostics and therapeutics. As demonstrated in this Account, nanoscaling laws for magnetic components are found to be critical to the design of optimized magnetic characteristics of hybrid nanoparticles and their enhanced applicability in the biomedical sciences including their utilizations as contrast enhancement agents for magnetic resonance imaging (MRI), ferromagnetic components for nano–bio hybrid structures, and translational vectors for magnetophoretic sensing of biological species. In particular, systematic modulation of saturation magnetization of nanoparticle probes is important to maximize MR contrast effects and magnetic separation of biological targets.

1. Introduction

The lodestone compass, the first invention utilizing magnetic materials, was critical in aiding 12th century explorers to navigate across unexplored parts of the world. Magnetic nanoparticles, the lodestone's miniature counterpart, can act as navigators or probes to similarly guide researchers as they seek to understand the deep inside of living objects. Many migratory animals and some

Published on the Web 02/19/2008 www.pubs.acs.org/acr
10.1021/ar700121f CCC: $40.75

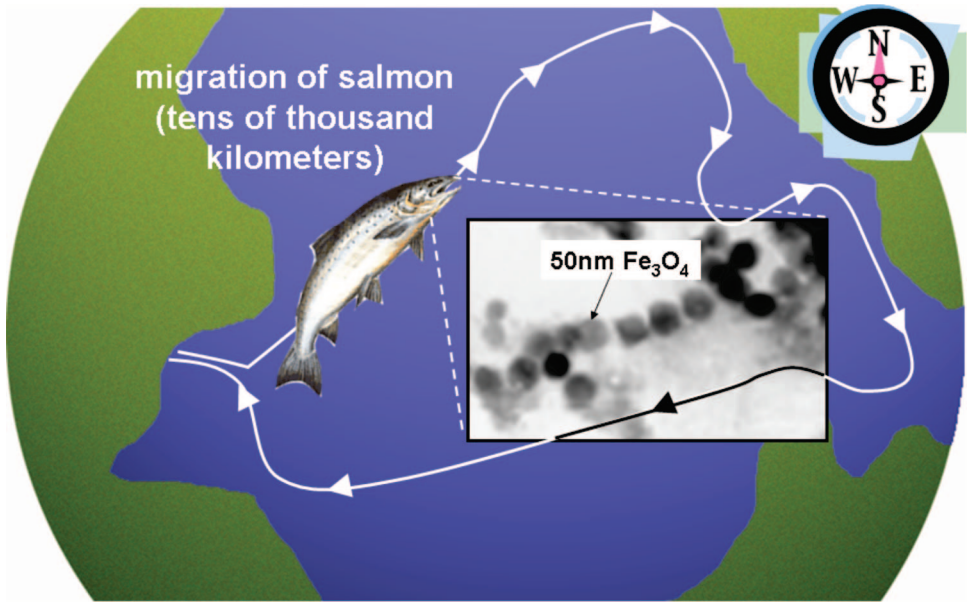

FIGURE 1. Magnetic nanoparticle-assisted natural navigation system used by salmon during migration. Reprinted with permission from *Nature* (http://www.nature.com), ref 1. Copyright 1997 Nature Publishing Group.

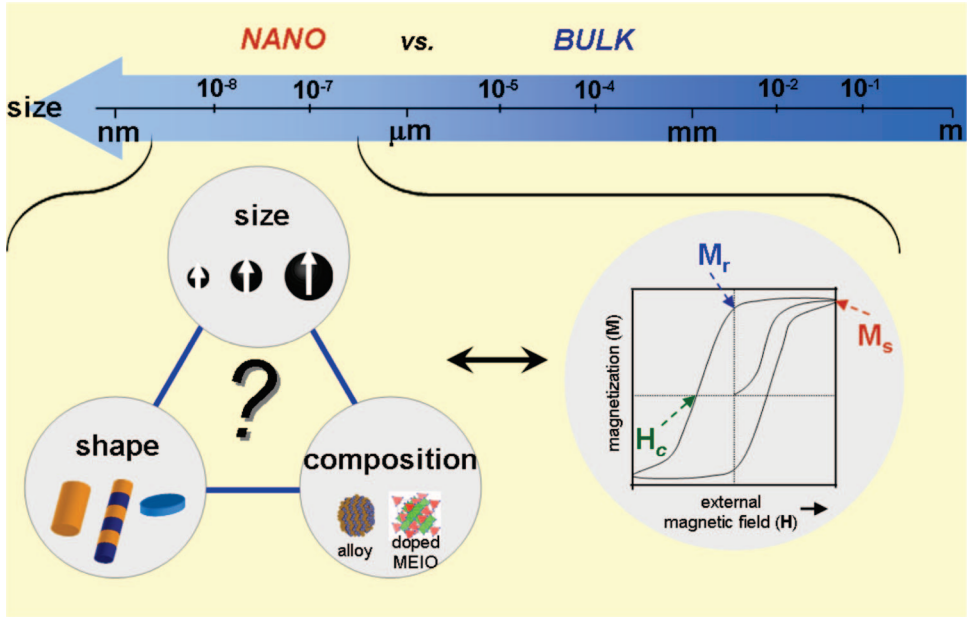

FIGURE 2. In nanometer scale, parameters such as size, shape, composition, and magnetocrystalline anisotropy strongly affect the magnetism (e.g., coercivity, mass magnetization, remanence) of nanoparticles.

microbes possess magnetic nanoparticles in their body that are utilized as a natural biomagnetic compass.[1] For example, salmon have a series of magnetic nanoparticles in the nasal capsules of their forehead, which are believed to respond to the geomagnetic field of the earth and help them reach their homes after journeys that can last tens of thousands of kilometers for three to four years (Figure 1).[1]

Scientists have developed artificial magnetic nanoparticles through chemical synthetic routes. In particular, recent progress in this field has yielded new types of magnetic nanoparticles with precisely tuned size, shape, and composition.[2−10] Many new interesting phenomena have been observed in these magnetic nanoparticles that are unique from their bulk counterparts. In addition to developing synthetic methods for these nanoparticles, understanding of their nanoscaling laws is also of great importance. The fundamental magnetic properties such as coercivity (H_c) and susceptibility (χ) are no longer permanent material characteristics and are susceptible to variations in their size, shape, and composition.[2,7,11−18] As a

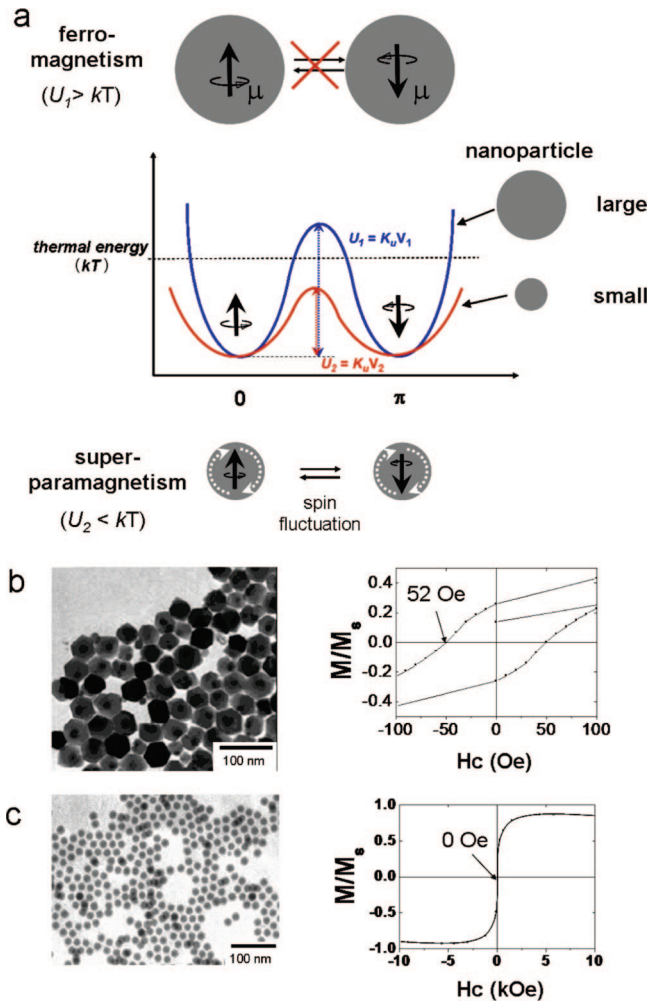

FIGURE 3. Nanoscale transition of magnetic nanoparticles from ferromagnetism to superparamagnetism: (a) energy diagram of magnetic nanoparticles with different magnetic spin alignment, showing ferromagnetism in a large particle (top) and superparamagentism in a small nanoparticle (bottom); (b, c) size-dependent transition of iron oxide nanoparticles from superparamagnetism to ferromagnetism showing TEM images and hysteresis loops of (b) 55 nm and (c) 12 nm sized iron oxide nanoparticles. Reproduced with permission from ref 9. Copyright 2004 American Chemical Society.

result, these scaling relationships can be used accordingly to tune magnetism from the ferromagnetic regime (unusually high magnetic energy product, $\mathbf{B}H_{max}$) to the superparamagnetic regime (zero coercivity in nanoscale regime).[15–18] Therefore, the nanoscaling laws of engineered magnetic nanoparticles are important not only to understand the behavior of existing materials but also to develop novel materials with superior properties.

Biomedical applications of such artificially engineered magnetic nanoparticles are promising since they can be useful as next-generation probes and vectors, which can significantly advance the current clinical diagnostic and therapeutic methods.[7,19–32] Upon conjugation with target-specific biomolecules, these magnetic nanoparticles can travel in human bodies via blood or lymphatic vessels and recognize desired biological targets and report their positions. Alternatively, by focusing an external magnetic field to the target region, magnetic nanoparticles can direct therapeutic agents to a localized target.

With such issues in mind, here we discuss the nanoscaling laws that determine the magnetic characteristics of artificially engineered nanoparticles. We will also address newly observed properties associated with these materials and describe their utilization as versatile and high performance probes for biomedical sciences.

2. Nanomagnetism Scaling Laws of Engineered Nanoparticles

In bulk materials, the key parameters for determining magnetic properties such as coercivity (H_c) and susceptibility (χ) are composition, crystallographic structure, magnetic anisotropic energy, and vacancies and defects.[33–36] However, when their size is decreased to the nanoscale regime, at least two more important parameters are strongly involved: size and shape (Figure 2).

2.1. Size Effects. One of the interesting size-dependent phenomena of nanoparticles is superparamagnetism. The magnetic anisotropic energy barrier from a spin-up state to spin-down state of the magnet is proportional to the product of the magnetic anisotropic constant (K_u) and the volume (V) of the magnet.[36] While bulk materials have magnetic anisotropic energies that are much larger than the thermal energy (kT) (Figure 3a (blue line)), the thermal energy of the nanoparticle is sufficient to readily invert the magnetic spin direction, although it is insufficient to overcome the spin–spin exchange coupling energy (Figure 3a (red line)). Such magnetic fluctuation leads to a net magnetization of zero, and this behavior is called superparamagnetism. The transition temperature from ferromagnetism to superparamagnetism is referred to as the blocking temperature (T_b) and is defined by the relationship $T_b = K_uV/25k$.[36] Such size-dependent magnetism changes can be observed in γ-Fe_2O_3 and cobalt nanoparticles.[9,12] γ-Fe_2O_3 nanoparticles of 55 nm exhibit ferrimagnetic behavior with a coercivity of 52 Oe at 300 K, but smaller 12 nm sized γ-Fe_2O_3 nanoparticles show superparamagnetism with no hysteresis behavior (Figure 3b,c). For cobalt nanoparticles, ferromagnetic to superparamagnetic transitions occur at much lower temperatures (T_b) of 10, 20, 100, 180, and 370 K for nanopar-

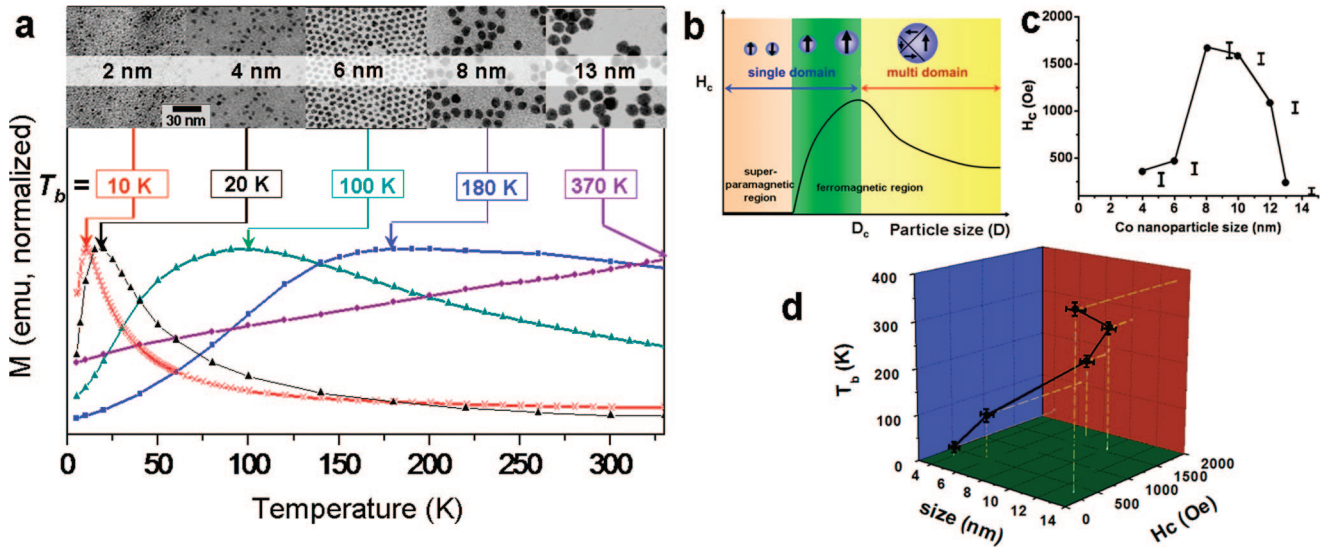

FIGURE 4. (a) Zero-field cooling curves and TEM images of Co nanoparticles with sizes of 2, 4, 6, 8, and 13 nm, (b) size-dependent magnetic domain structures from superparamagnetism to single domain and multidomain ferromagnetism, (c) size-dependent coercivity of Co nanoparticles, and (d) plot of H_c and T_b vs size of Co nanoparticles. Reproduced with permission from ref 7 (Figure 4a) and ref 12 (Figure 4b–4d). Copyright 2007 Royal Society for Chemistry and Copyright 2002 Wiley-VCH.

ticles with sizes of 2, 4, 6, 8, and 13 nm, respectively, in comparison to 1394 K for bulk cobalt (Figure 4a).

Nanoparticle size effects can also be observed in changes in magnetic coercivity (H_c). In contrast to the bulk magnet, which possesses multiple magnetic domain structures, nanoparticles possess single magnetic domain structures below a certain critical size (D_c) where all magnetic spins in the nanoparticle align unidirectionally (Figure 4b). In this single-domain regime, the magnetic coercivity increases as the size of the nanoparticle increases with the relationship $H_c = 2K_u/m_s[1 - 5(kT/K_uV)^{1/2}]$ where m_s is the saturation magnetization.[36] Above the critical size ($D > D_c$), multidomain magnetism begins in which a smaller reversal magnetic field is required to make the net magnetization zero. In the case of Co nanoparticles, the magnetic coercivity increases from 370 to 1680 Oe in a single-domain regime as the size of the Co nanoparticles increases from 4 to 8 nm (Figure 4c).[12] However, the magnetic coercivity decreases to 1600, 1100, and 250 Oe as the size of the Co nanoparticles further increases to 10, 12, and 13 nm by forming multimagnetic domains (Figure 4c). Therefore, the critical single-domain size of Co nanoparticles is expected to be around 8–10 nm. From such size-dependent properties of cobalt nanoparticles, a graph of scaling laws of cobalt nanoparticles on coercivity and blocking temperature is shown in Figure 4d.

Saturation magnetization of nanoparticles is also strongly dependent on their size. Intrinsically, magnetic materials possess magnetically disordered spin glass like layers near the surface due to the reduced spin–spin exchange coupling energy at the surface.[37,38] In bulk cases, since the disordered surface layer is minimal compared with the total volume of the magnet, such surface spin canting effects are negligible. Upon reduction of the size of magnetic materials to nanoscale regime, however, the surface canting effects are dramatically pronounced in the saturation magnetization value (m_s), described as

$$m_s = M_S[(r - d)/r]^3 \quad (1)$$

where r is the size, M_S is the saturation magnetization of bulk materials, and d is the thickness of disordered surface layer.[37] For very small nanoparticles less than ~5 nm, such size effect on m_s is more noticeable, since internal spins of the nanoparticle also start to be canted as well as the surface spins due to increased interactions between the surface and internal spins.[37]

Such size effects on magnetization have been well demonstrated in the case of magnetism-engineered iron oxide (MEIO), Fe_3O_4, nanoparticles.[13] As the size of MEIO nanoparticles increases from 4 to 6, 9, and 12 nm, the mass magnetization values change from 25 to 43, 80, and 101 emu/(g Fe), respectively (Figure 5a). This result shows a linear relationship upon the plotting of $m_s^{1/3}$ vs r^{-1} (Figure 5b) as predicted in eq 1. Such size-dependent mass magnetization values directly affect their magnetic resonance (MR) signal enhancement capabilities for molecular imaging of biological targets (*vide infra*).

2.2. Shape and Composition Effects on Nanomagnetism. The anisotropic constant (K_u) is known to be strongly correlated with various anisotropies such as shape, magne-

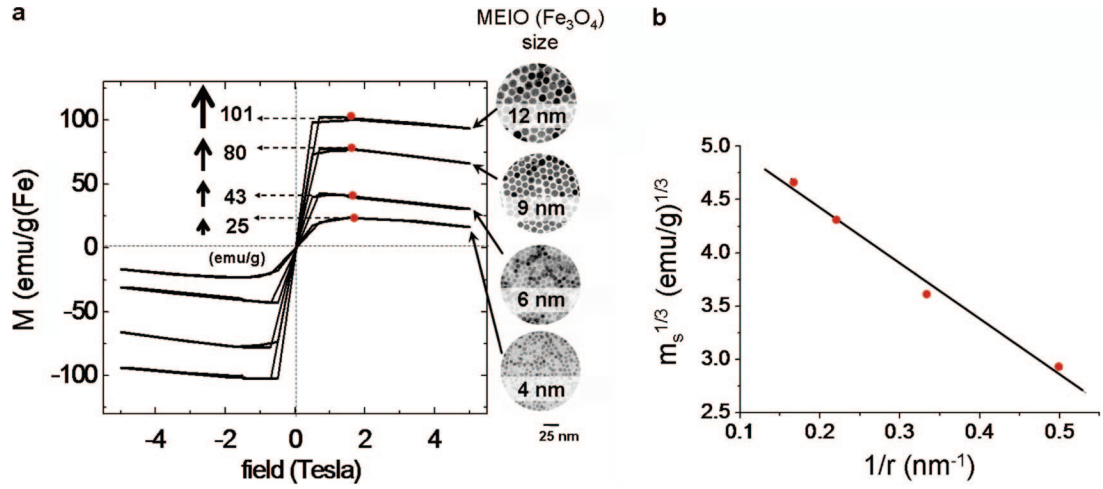

FIGURE 5. Size dependent mass magnetization values of 4, 6, 9, and 12 nm magnetism-engineered iron oxide (MEIO) nanoparticles: (a) hysteresis loops, mass magnetization values at 1.5 T, and TEM images; (b) plot of $m_s^{1/3}$ vs r^{-1}. Reproduced with permission from ref 13. Copyright 2005 American Chemical Society.

tocrystalline, and exchange.[33–36] For example, shape anisotropy of particles is expressed as

$$K_u = [H_a + (N_2 - N_1)M_s]M_s/2 \quad (2)$$

where H_a is the anisotropy field and N_2 and N_1 are the demagnetization factors parallel and perpendicular to the easy axis of the magnetic particle.[36] Such effects can be observed in CoPt barcode-structured nanowires with various aspect ratios.[39] The aspect ratios ($\gamma = b/a$) of Co bar fragments are tuned by controlling their length (b) with a fixed diameter (a) of 65 nm (Figure 6a–d). For Co nanowires with a high aspect ratio ($\gamma = 45$), the coercivity of the nanowire magnetized along the b direction ($H_{c(b)}$) is 668 Oe (Figure 6e (red line)). As γ is decreased to 3.5, 1, and 0.25, the coercivity of the sample decreases to 667, 164, and 76 Oe, respectively (Figure 6f–h (red lines),i (red squares)), indicating that higher γ (i.e., larger shape anisotropy) of the Co bar fragments leads to the larger magnetic coercivity. Such shape anisotropy effects can be also observed upon changes in the direction of the external magnetic field. For nanowires with rod-shaped Co bar fragments ($\gamma = 45$ or 3.5), larger magnetic coercivities are obtained from nanowires magnetized along the b direction ($H_{c(b)}$) than from nanowires magnetized along the a direction ($H_{c(a)}$) (Figure 6e,f,i). In contrast, nanowires with disk-shaped Co bar fragments (i.e., $\gamma = 1$ or 0.25) have higher $H_{c(a)}$ than $H_{c(b)}$ (Figure 6g–i). Such results indicate that the magnetically easy axis of the nanowires changes from b direction to a direction due to shape anisotropy effects as the shape of the Co bar fragments varies from rods to discs.

The magnetocrystalline phase of the nanoparticle is significant in determining the magnetic coercivity of the nanoparticle.[15–18] This can be observed in magnetic nanoalloys with anisotropic crystalline structures. Co@Pt core–shell nanoparticles composed of an isotropically structured face-centered cubic (fcc) Co core and a nonmagnetic Pt shell exhibit superparamagnetic behavior with zero coercivity at room temperature (Figure 7a,b,d).[15–17] However, after thermal treatment, they transform to anisotropically structured face-centered tetragonal (fct) CoPt nanoalloys (Figure 7a,c), which now exhibit room-temperature ferromagnetic behavior with a coercivity value of 5300 Oe due to large magnetocrystalline anisotropy (Figure 7e).[16]

Compositional modification of nanoparticles by the adoption of magnetic dopants can significantly change the magnetism of nanoparticles.[14] For example, magnetism-engineered iron oxide (MEIO), Fe_3O_4, nanoparticles have a ferrimagnetic spin structure where Fe^{2+} and Fe^{3+} occupying O_h sites align parallel to the external magnetic field and Fe^{3+} in the T_d sites of fcc-packed oxygen lattices align antiparallel to the field (Figure 8a). Since Fe^{3+} possesses a d^5 electron configuration with a high spin state and Fe^{2+} has a d^6 configuration with a high spin state, the total magnetic moment per unit $(Fe^{3+})_{T_d}(Fe^{2+}Fe^{3+})_{O_h}O_4$ is approximately $4\mu_B$. Incorporation of a magnetic dopant M^{2+} (M = Mn, Co, Ni) with electron configurations of d^5, d^4, and d^3, respectively, to replace O_h Fe^{2+} leads to change in the net magnetization (Figure 8b). The magnetic moment per unit $MnFe_2O_4$ (Mn-MEIO), $CoFe_2O_4$ (Co-MEIO), and $NiFe_2O_4$ (Ni-MEIO) is now estimated as $5\mu_B$, $3\mu_B$, and $2\mu_B$, respectively. Due to such compositional effects, the experimentally observed mass magnetization value at 1.5 T gradually decreases from 110 emu to 101, 99, and 85

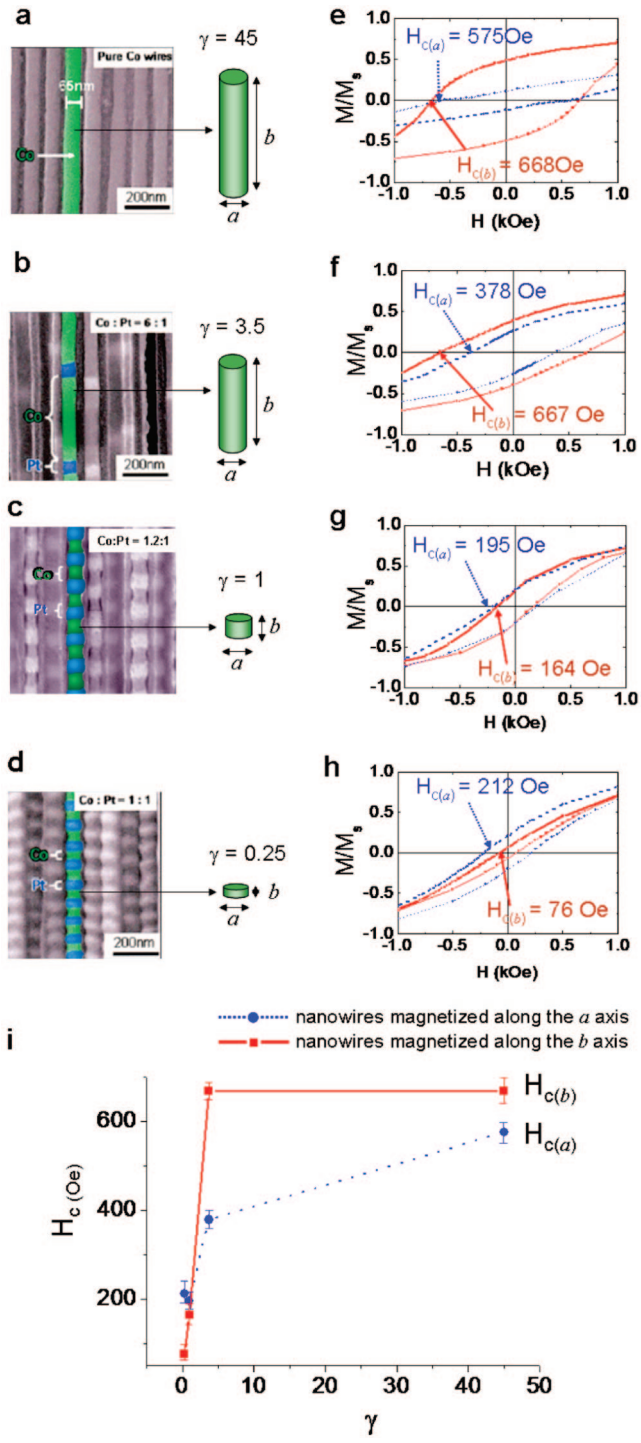

FIGURE 6. Scanning electron microscopic (SEM, a–d) images of CoPt barcodes with various aspect ratio (γ) of Co bars and their shape-dependent magnetism (e–h) under parallel (i.e., *b* axis) and perpendicular (i.e., *a* axis) magnetic fields with respect to the nanowire direction and (i) plot of coercivity ($H_{c(a)}$, $H_{c(b)}$) vs γ. Reproduced with permission from ref 39. Copyright 2005 American Chemical Society.

emu per mass of magnetic atoms (emu/g(M+Fe)) for Mn-MEIO, MEIO, Co-MEIO, and Ni-MEIO, respectively (Figure 8c).[14]

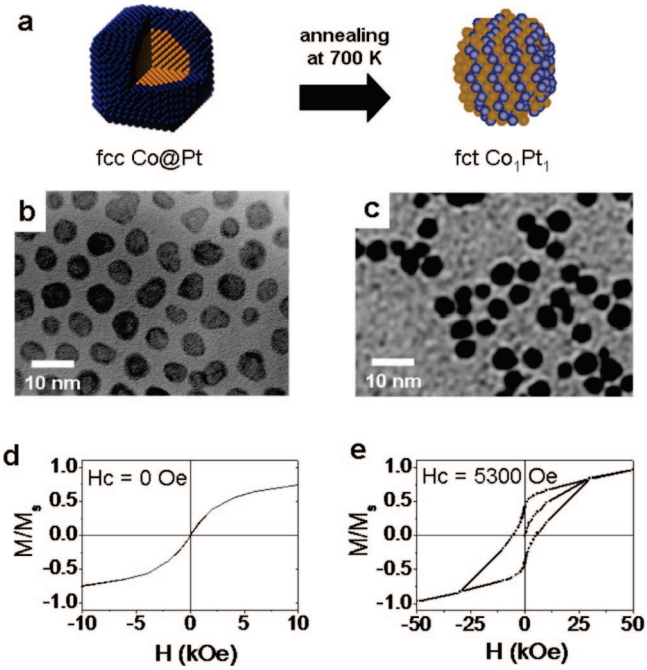

FIGURE 7. Magnetocrystalline phase effects on magnetism: (a) schematic of ferromagnetic phase transition of fcc Co@Pt core–shell nanoparticles to fct CoPt nanoalloys; TEM images and hysteresis loops of (b, d) fcc Co@Pt core–shell nanoparticles and (c, e) fct CoPt nanoalloys. Reproduced with permission from ref 16. Copyright 2004 American Chemical Society.

3. Magnetism-Engineered Nanoparticles for Biomedical Applications

Attaining the specific targeting ability of magnetic nanoparticles is important for their biomedical applications. This can be achievable by tailoring nanoparticle surface with appropriate ligands, which can endow high colloidal and biostability, low nonspecific binding affinity, and facile bioconjugation with target-specific chemical and biological molecules.

3.1. Magnetic Resonance Imaging of Biological Targets. Magnetic nanoparticles provide strong contrast effects on surrounding tissues under MRI scans and therefore have served as important probes for MR imaging. MR contrast effects of magnetic nanoparticles can be simply understood in terms of their effect on the spin–spin relaxation time of surrounding water protons. Conventional iron oxide based contrast agents such as superparamagnetic iron oxide (SPIO) and related nanoparticle probes (e.g., cross-linked iron oxide (CLIO)) have limited uses for advanced MR imaging due to their relatively poor magnetic contrast effects (i.e., low magnetic moment and also low r_2 coefficient).[25,40,41] Therefore, a new type of magnetic nanoparticles such as MEIO with high and tunable mass magnetization values are needed to enhance the relaxation process of the proton nuclear spins.[42]

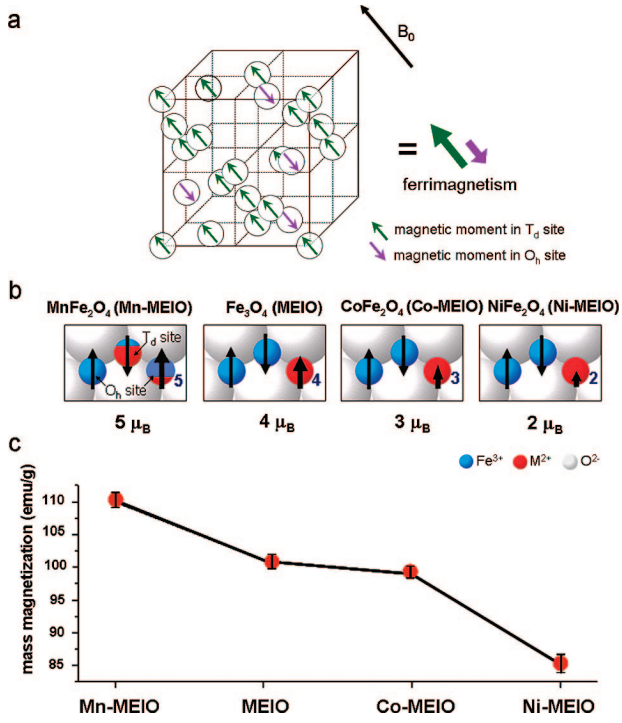

FIGURE 8. (a) Ferrimagnetic spin structure of inverse spinel ferrites and (b) schematic spin moments and (c) mass magnetization values of various metal-doped MEIO nanoparticles (MFe_2O_4, M = Mn, Fe, Co, Ni). Reprinted with permission from *Nature Medicine* (www.nature.com), ref 14. Copyright 2007 Nature Publishing Group.

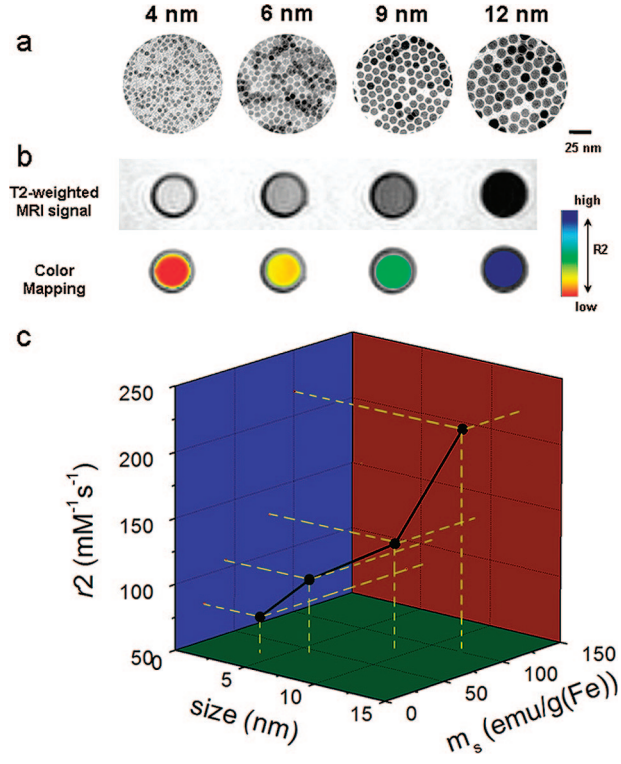

FIGURE 9. Nanoscale size effects of MEIO nanoparticles on MR contrast effects: (a) TEM images; (b) MR images and their color maps; (c) plot of m_s and r_2 values vs size of 4, 6, 9, and 12 nm MEIO. Reproduced with permission from ref 13. Copyright 2005 American Chemical Society.

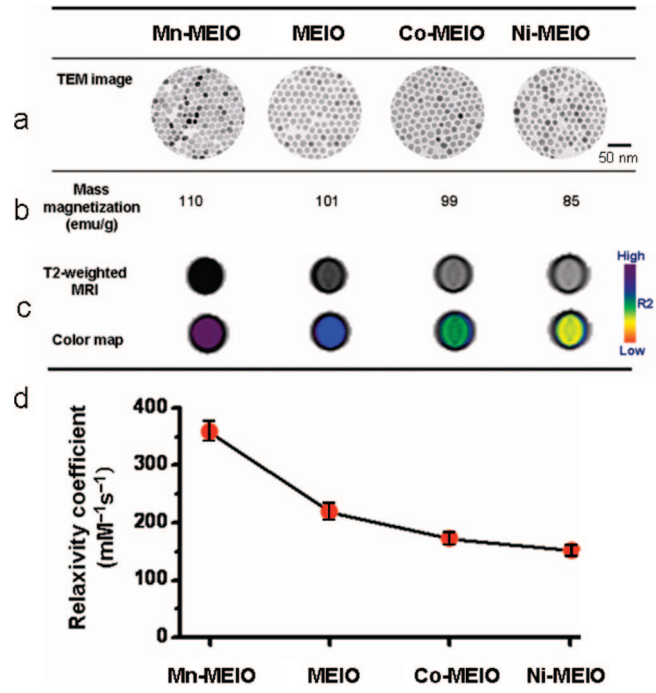

FIGURE 10. Composition effects of metal-doped MEIO nanoparticles: (a) TEM images; (b) mass magnetization values; (c) MR images and their color maps; (d) relaxivity coefficient (r_2) values of Mn-MEIO, MEIO, Co-MEIO, and Ni-MEIO. Reprinted with permission from *Nature Medicine* (www.nature.com), ref 14. Copyright 2007 Nature Publishing Group.

In particular, significant shortening of the spin–spin relaxation time (T_2) of the proton is possible by using a new type of magnetic nanoparticles.

As described in section 2.1, larger MEIO nanoparticles possess higher magnetization values and exhibit stronger MR contrast effects, which are observed as darker MR contrast and blue in color MRI maps (Figure 9a,b).[13] The relaxivity coefficient (r_2), which is a direct indication of contrast enhancement effects, is 78 mM^{-1} s^{-1} for 4 nm MEIO and gradually increases to 106, 130, and to 218 mM^{-1} s^{-1} for 6, 9, and 12 nm size MEIO nanoparticles (Figure 9c).

In addition to the size effects, magnetic dopant effects of MEIO nanoparticles are also significant. For example, Mn-MEIO nanoparticles with the highest magnetization values of 110 emu/g(Mn+Fe) exhibit the best MR signal enhancement effects with an r_2 of 358 mM^{-1} s^{-1} (Figure 10).[14] Other metal-doped MEIO nanoparticles including MEIO, Co-MEIO, and Ni-MEIO with diminished mass magnetization values of 101 emu/g(Fe), 99 emu/g(Co+Fe), and 85 emu/g(Ni+Fe), respectively, show less MR contrast effects with r_2 of 218, 172, and 152 mM^{-1} s^{-1}, respectively, which is consistent with the trend of mass magnetization of nanoparticles (Figure 10). It is noteworthy that the r_2 of 12 nm Mn-MEIO nanoparticles is ~5.8 times higher than that of conventional molecular MR imaging contrast agents such as cross-linked iron oxide (CLIO) nanoparticles.

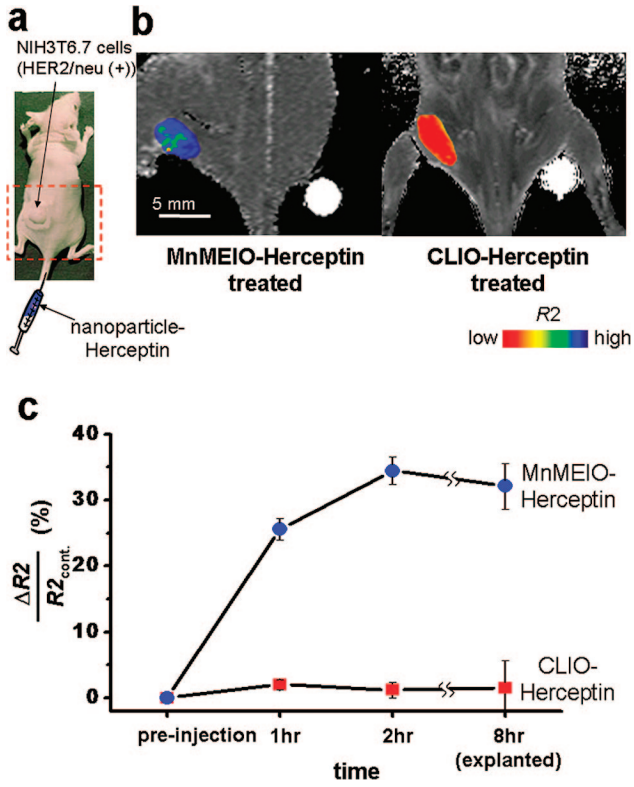

FIGURE 11. Ultrasensitive *in vivo* cancer detection through the utilization of Mn-MEIO−Herceptin nanoparticle probes: (a) tail vein injection of the Mn-MEIO−Herceptin probes into a mouse with a small (~50 mg) HER2/neu positive cancer in its proximal femur region; (b) color-mapped MR images of the mouse treated with Mn-MEIO−Herceptin conjugates; (c) time-dependent R_2 changes at the tumor site after injection of Mn-MEIO−Herceptin probes (blue circle) and CLIO−Herceptin probes (red square). Reprinted with permission from *Nature Medicine* (www.nature.com), ref 14. Copyright 2007 Nature Publishing Group.

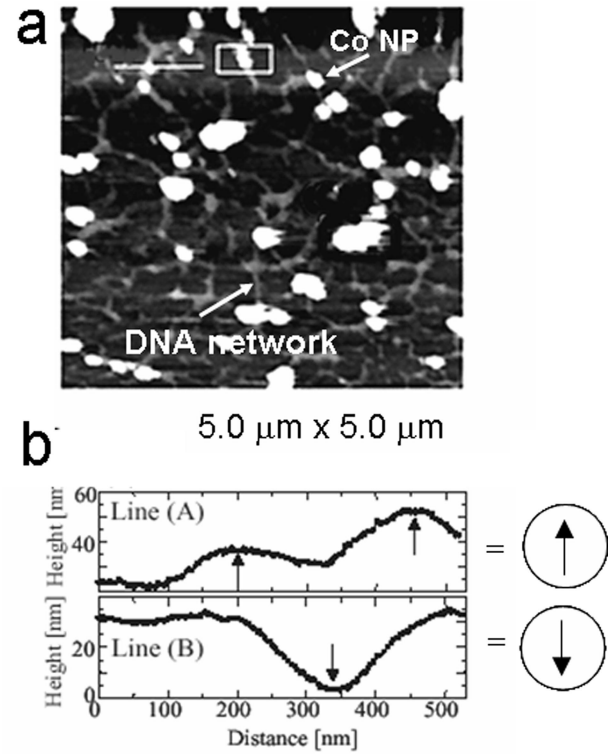

FIGURE 12. (a) Atomic force microscopic images of a DNA−Co nanoparticle hybrid network structure and (b) magnetic force microscopic scanning of a single Co nanoparticle with either parallel (top) or reversal (bottom) spin directions located in different regions. Reproduced from ref 45 with permission. Copyright 2002 American Scientific Publishers.

Such MR signal enhancement effects of Mn-MEIO nanoparticles enable successful ultrasensitive *in vivo* detection of biological targets.[14] When these molecules are conjugated with a cancer-targeting antibody, Herceptin, and intravenously injected into a mouse with a small HER2/neu positive cancer (~50 mg), they selectively detect small cancer with strong MR signals shown as blue color, which represents high MR relaxivity ($R_2 = 1/T_2$)) (Figure 11a,b). In contrast, there is no noticeable MR signal change ($\Delta R_2/R_{2,\text{control}}$) at the cancer region from the mouse treated with conventional CLIO−Herceptin conjugates (Figure 11b,c).

3.2. Ferromagnetic Magnet−DNA Network Structures. Self-assembly of biomolecules to form highly ordered and programmed three-dimensional structures through specific molecular recognition and biological interactions such as protein−protein interaction, DNA hybridization, hydrogen bonding, and van der Waals forces has been observed.[43,44] In particular, DNA is a naturally occurring biopolymer with sequence-specific self-assembly capabilities. By engineering DNA sequences, it is possible to form various DNA nanoarchitectures such as multimers, wires, and networks. Therefore, DNA molecules can serve as templates for making magnetic nanoparticle assemblies. For example, hybridization of ferromagnetic Co nanoparticles with DNA induces the formation of magnetic nanoparticle network structures.[45] Based on the nanoscaling laws described in section 2.1, Co nanoparticles show single-domain ferromagnetic behaviors around 10 nm. When ferromagnetic 12 nm Co nanoparticles coated with 2-mercaptoethylamine hydrochloride are mixed with poly(C)·poly(G) single-stranded DNA (ssDNA), Co nanoparticles on double-stranded DNA (dsDNA) network structures are formed due to the electrostatic interaction between positively charged nanoparticles and negatively charged dsDNA networks (Figure 12a). Magnetic force microscopic (MFM) images of these magnet−DNA network structures show that the nanoparticles have both up-spin and down-spin states like "bits" in magnetic data storage (Figure 12b). Furthermore, such a ferromagnetic−bio hybrid system can be potentially useful for the detection of biological events such as DNA hybridization and cleavage via MFM or superconducting quantum interference device (SQUID) sensors.

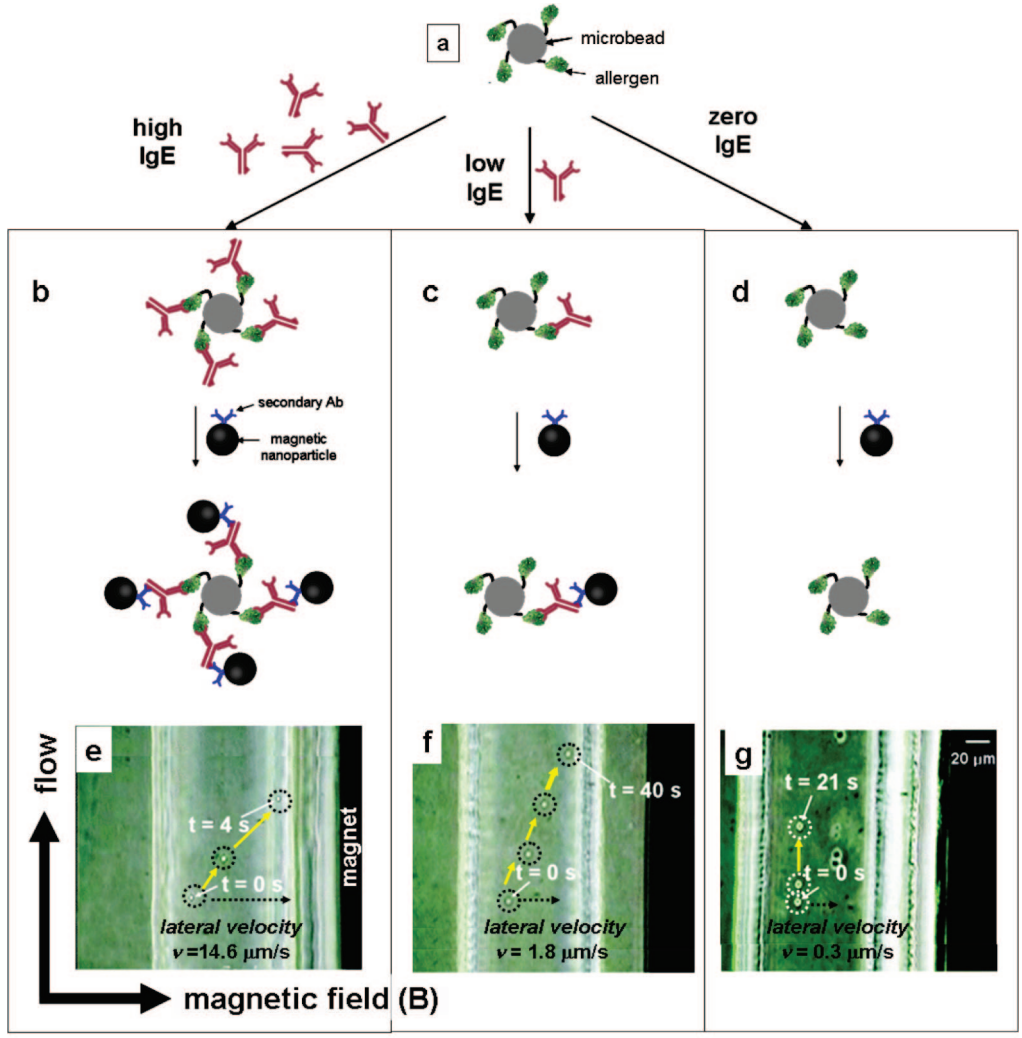

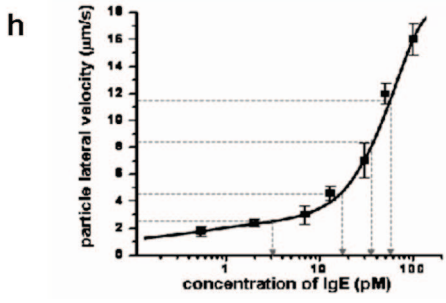

i

IgE quantification of patients

patient number	microbead velocity (μm/s)	concn. of IgE from the standard curve (pM)
1	2.531	4.89
2	11.69	34.68
3	8.215	21.4
4	4.45	12.05

FIGURE 13. Magnetophoretic sensing of allergen-specific IgE: (a) microbeads coated with allergen; detection scheme at (b) high, (c) low, and (d) zero concentration of the target IgE; (e–g) magnetophoretic movements of the samples shown in panels b–d; (h) standard calibration curve of particle lateral velocity vs IgE concentration; (i) quantification of target IgE in sera of patients calculated by the standard curve in panel h. Reproduced with permission from ref 49. Copyright 2007 American Chemical Society.

3.3. Magnetophoretic Biosensing and Separation. Magnetophoretic sensing and separation of biological targets can also be accomplished by using magnetic particles. When an external magnetic field is applied perpendicular to the flow direction of a microfluidic channel, magnetic particles experience a magnetic force (*F*), which drives their magnetophoretic lateral movement with a velocity of v_{lat}.

$$v_{lat} = \frac{2\Delta\chi r^2}{9\eta\mu_0}(\nabla\vec{B}) \cdot \vec{B} \qquad (3)$$

where $\Delta\chi$ is magnetic susceptibility of the particle, r is the particle radius, μ_0 is the vacuum permeability, and B is the external magnetic field.[46]

Magnetic beads have been widely used for such magnetic sensing and separation purposes, but these still have problems including low magnetic susceptibility and magnetic inhomogeniety.[46−48] By use of nanoparticles with well-defined size and magnetism, however, ultrasensitive and reliable allergen-specific IgE detection is possible.[49] Magnetic susceptibility of nanoparticles plays an important role in the velocity control and subsequent biological target separations as predicted by eq 3. Allergies are caused by a hypersensitive reaction between allergens and allergen-specific IgE antibodies. Allergen-specific IgE can be found in the serum of the allergy patient, but its concentration is very low, and therefore highly sensitive detection of IgE is important.[50] Microbeads coated with mite allergen from *Dermatophagoides farinae* (Figure 13a) are first mixed with the target IgE with varying concentrations. Then anti-human IgE-coated MEIO nanoparticles with the capability to bind to the Fc region of the target IgE are further added, and the resulting solution is injected into the microfluidic channel. At a high concentration of the target IgE, significant lateral movement of microbeads with a velocity (v_{lat}) of ∼15 μm/s is observed (Figure 13b,e), while reduced (v_{lat} = ∼2 μm/s) and negligible lateral movements are seen at lower concentrations of IgE or no IgE, respectively (Figure 13c,d,f,g). Such observations are reasonable since the higher IgE concentrations induce more binding of MEIO nanoparticles onto the microbeads. Quantitative detection of the target IgE in sera is also possible up to subpicomolar IgE levels (∼500 fM) by using a target IgE concentration vs lateral velocity standard calibration curve (Figure 13h,i).

4. Concluding Remarks

In this Account, we have discussed the nanoscaling laws of magnetic nanoparticles and reviewed selected case studies on metal, metal ferrite, and metal alloy nanoparticles. In the size range of 1−50 nm, parameters including size, shape, and composition have a tremendous influence on magnetic characteristics such as coercivity and magnetization values. Such scaling laws of magnetic nanoparticles can make them programmable for their ultimate performance for specific biomedical applications, as demonstrated in their utilization as superior MR contrast agents and magnetic separation vectors. Although the current understanding of nanoscaling laws of magnetism is still limited, more studies and experimental exploration into this area of nanomagnetism can lead to significant advances in various fields of next-generation biomedical sciences such as drug delivery, hyperthermia, MRI, magnetic separation and biosensors, and nanobiofunctional magnetic materials.

This research is supported by the Korea Research Council of Fundamental Science & Technology, the National Research Laboratory (Grant M1060000255), Nano-Bio Science & Technology Program (Grant M1050300218-05M0300-21810), NCRC (Grant R15-2004-024-02002-0), NCI Center for Cancer Nanotechnology Excellence (CCNE), NBIT (Grant K20716000001-07A0400-00110), and 2nd stage BK21 for Chemistry.

BIOGRAPHICAL INFORMATION

Young-wook Jun received his B.S. degree from Yonsei University and Ph.D. degree from the Korea Advanced Institute of Science and Technology in 2005, where he studied the synthetic and mechanistic aspects of nanocrystals. After a postdoctoral training on nanoparticle-assisted MRI at Yonsei University with Professor Cheon, he is currently working on the nanoparticle-assisted single molecule spectroscopy of biological phenomena with Professor Alivisatos at the University of California, Berkeley.

Jung-wook Seo received his B.S. and M.S. degrees from Seoul National University and his Ph.D. degree from Yonsei University in 2007. His thesis was focused on the development of metal oxide and metal chalcogenide nanocrystals. He is a senior scientist at Samsung-Electromechanics where he works in the field of surface metalization and nanoparticle researches for electronic devices.

Jinwoo Cheon is the director of Convergence Nanomaterials National Research Laboratory of Korea. He graduated from Yonsei University with B.S. and received his Ph.D. from University of Illinois, Urbana−Champaign in 1993. After postdoctoral training at U.C. Berkeley and also at UCLA, he joined the KAIST where he was an assistant and then associate professor. In 2002, he moved to Yonsei University. His research interests include the development of functional inorganic nanoparticles and their biomedical and energy related applications.

FOOTNOTES

*To whom correspondence should be addressed. E-mail: jcheon@yonsei.ac.kr.

REFERENCES

1 Walker, M.; Diebel, C.; Haugh, C.; Pankhurst, P.; Montgomery, J.; Green, C. Structure and function of the vertebrate magnetic sense. *Nature* **1997**, *390*, 371–376.

2 Murray, C. B.; Sun, S. H.; Doyle, H.; Betley, T. Monodisperse 3d transition-metal (Co, Ni, Fe) nanoparticles and their assembly into nanoparticle superlattices. *MRS Bull.* **2001**, *26*, 985–991.

3 Sun, S. H.; Zeng, H.; Robinson, D. B.; Raoux, S.; Rice, P. M.; Wang, S. X.; Li, G. X. Monodisperse MFe_2O_4 (M = Fe, Co, Mn) nanoparticles. *J. Am. Chem. Soc.* **2004**, *126*, 273–279.

4 Sun, S. H. Recent advances in chemical synthesis, self-assembly, and applications of FePt nanoparticles. *Adv. Mater.* **2006**, *18*, 393–403.

5 Hyeon, T. Chemical synthesis of magnetic nanoparticles. *Chem. Commun.* **2003**, 927–934.

6 Jana, N. R.; Chen, Y.; Peng, X. Size- and shape-controlled magnetic (Cr, Mn, Fe, Co, Ni) oxide nanocrystals via a simple and general approach. *Chem. Mater.* **2004**, *16*, 3931–3935.

7 Jun, Y.; Choi, J.; Cheon, J. Heterostructured magnetic nanoparticles: Their versatility and high performance capabilities. *Chem. Commun.* **2007**, 1203–1214.

8 Park, J.; An, K. J.; Hwang, Y. S.; Park, J. G.; Noh, H. J.; Kim, J. Y.; Park, J. H.; Hwang, N. M.; Hyeon, T. Ultra-large scale synthesis of monodispersed nanocrystals. *Nat. Mater.* **2004**, *3*, 891–895.

9 Cheon, J.; Kang, N.-J.; Lee, S.-M.; Yoon, J.-H.; Oh, S. J. Shape evolution of single-crystalline iron oxide nanocrystals. *J. Am. Chem. Soc.* **2004**, *126*, 1950–1951.

10 Shevchenko, E. V.; Talapin, D. V.; Rogach, A. L.; Kornowski, A.; Haase, M.; Weller, H. Colloidal synthesis and self-assembly of $CoPt_3$ nanocrystals. *J. Am. Chem. Soc.* **2002**, *124*, 11480–11485.

11 Leslie-Pelecky, D. L.; Rieke, R. D. Magnetic properties of nanostructured materials. *Chem. Mater.* **1996**, *8*, 1770–1783.

12 Park, J.-I.; Kang, N.-J.; Jun, Y.; Oh, S. J.; Ri, H. C.; Cheon, J. Superlattice and magnetism directed by the size and shape of nanocrystals. *ChemPhysChem* **2002**, *3*, 543–547.

13 Jun, Y.; Huh, Y.-M.; Choi, J.-s.; Lee, J.-H.; Song, H.-T.; Kim, S. J.; Yoon, S.; Kim, K.-S.; Shin, J.-S.; Suh, J.-S.; Cheon, J. Nanoscale size effect of magnetic nanocrystals and their utilization for cancer diagnosis via magnetic resonance imaging. *J. Am. Chem. Soc.* **2005**, *127*, 5732–5733.

14 Lee, J.-H.; Huh, Y.-M.; Jun, Y.; Seo, J.-w.; Jang, J.-t.; Song, H.-T.; Kim, S. J.; Cho, E.-J.; Yoon, H.-G.; Suh, J.-S.; Cheon, J. Artificially engineered magnetic nanoparticles for ultra-sensitive molecular imaging. *Nat. Med.* **2007**, *13*, 95–99.

15 Park, J.-I.; Cheon, J. Synthesis of "solid solution" and "core−shell" type cobalt−platinum magnetic nanoparticles via transmetalation reactions. *J. Am. Chem. Soc.* **2001**, *123*, 5743–5746.

16 Park, J.-I.; Kim, M. G.; Jun, Y.; Lee, J. S.; Lee, W.-r.; Cheon, J. Characterization of superparamagnetic "core-shell" nanoparticles and monitoring their anisotropic phase transition to ferromagnetic "solid solution" nanoalloys. *J. Am. Chem. Soc.* **2004**, *126*, 9072–9078.

17 Lee, W.; Kim, M. G.; Choi, J.; Park, J. I.; Ko, S. J.; Oh, S. J.; Cheon, J. Redox-transmetalation process as a generalized synthetic strategy for core-shell magnetic nanoparticles. *J. Am. Chem. Soc.* **2005**, *127*, 16090–16097.

18 Sun, S.; Murray, C. B.; Weller, D.; Folks, L.; Moser, A. Monodisperse FePt nanoparticles and ferromagnetic FePt nanocrystal superlattices. *Science* **2000**, *287*, 1989–1992.

19 Mirkin, C. A.; Niemeyer, C. M. *Nanobiotechnology II: More Concept and Applications*; Wiley-VCH: Weinheim, Germany, 2007.

20 Huh, Y.-M.; Jun, Y.; Song, H.-T.; Kim, S. J.; Choi, J.-s.; Lee, J.-H.; Yoon, S.; Kim, K.-S.; Shin, J.-S.; Suh, J.-S.; Cheon, J. In vivo magnetic resonance detection of cancer by using multifunctional magnetic nanocrystals. *J. Am. Chem. Soc.* **2005**, *127*, 12387–12391.

21 Xu, C.; Xu, K.; Gu, H.; Zheng, R.; Liu, H.; Zhang, X.; Guo, Z.; Xu, B. Dopamine as a robust anchor to immobilize functional molecules on the iron oxide shell of magnetic nanoparticles. *J. Am. Chem. Soc.* **2004**, *126*, 9938–9939.

22 Son, S. J.; Reichel, J.; He, B.; Schuchman, M.; Lee, S. B. Magnetic nanotubes for magnetic-field-assisted bioseparation, biointeraction, and drug delivery. *J. Am. Chem. Soc.* **2005**, *127*, 7316–7317.

23 Weissleder, R.; Moore, A.; Mahmood, U.; Bhorade, R.; Benveniste, H.; Chiocca, E. A.; Basilion, J. P. In vivo magnetic resonance imaging of transgene expression. *Nat. Med.* **2000**, *6*, 351–355.

24 Lewin, M.; Carlesso, N.; Tung, C. H.; Tang, X. W.; Cory, D.; Scadden, D. T.; Weissleder, R. Tat peptide-derivatized magnetic nanoparticles allow in vivo tracking and recovery of progenitor cells. *Nat. Biotechnol.* **2000**, *18*, 410–414.

25 Pankhurst, Q. A.; Connolly, J.; Jones, S. K.; Dobson, J. Applications of magnetic nanoparticles in biomedicine. *J. Phys. D* **2003**, *36*, R167–R181.

26 Jordan, A.; Scholz, R.; Wust, P.; Fahling, H.; Felix, R. Magnetic fluid hyperthermia (MFH): Cancer treatment with AC magnetic field induced excitation of biocompatible superparamagnetic nanoparticles. *J. Magn. Magn. Mater.* **1999**, *201*, 413–419.

27 Bulte, J. W. M.; Kraitchman, D. L. Iron oxide MR contrast agents for molecular and cellular imaging. *NMR Biomed.* **2004**, *17*, 484–499.

28 Ferrari, M. Cancer nanotechnology. Opportunities and challenges. *Nat. Rev. Cancer* **2005**, *5*, 161–171.

29 Kim, J.; Park, S.; Lee, J. E.; Jin, S. M.; Lee, J. H.; Lee, I. S.; Yang, I.; Kim, J. S.; Kim, S. K.; Cho, M. H.; Hyeon, T. Designed fabrication of multifunctional magnetic gold nanoshells and their application to magnetic resonance imaging and photothermal therapy. *Angew. Chem., Int. Ed.* **2006**, *45*, 7754–7758.

30 Rosi, N.; Mirkin, C. Nanostructures in biodiagnostics. *Chem. Rev.* **2005**, *105*, 1547–1562.

31 Stoeva, S. I.; Huo, F. W.; Lee, J. S.; Mirkin, C. A. Three-layer composite magnetic nanoparticle probes for DNA. *J. Am. Chem. Soc.* **2005**, *127*, 15362–15363.

32 Harisinghani, M. G.; Barentsz, J.; Hahn, P. F.; Deserno, W. M.; Tabatabaei, S.; van de Kaa, C. H.; de la Rosette, J.; Weissleder, R. Noninvasive detection of clinically occult lymph-node metastases in prostate cancer. *N. Eng. J. Med.* **2003**, *348*, 2491–2505.

33 Cullity, B. D. *Introduction to Magnetic Materials*; Addison-Wesley Publishing: Reading, MA, 1972.

34 McCurrie, R. A. *Ferromagnetic Materials: Structure and Properties*; Academic Press, San Diego, CA, 1994.

35 Cornell, R. M.; Schwertmann, U. *The Iron Oxides*; Wiley-VCH: Weinheim, Germany, 2003.

36 Jales, D. *Introduction to Magnetism and Magetnic Materials*; CRC Press, Boca Raton, FL, 1998.

37 Morales, M. P.; Veintemillas-Verdaguer, S.; Montero, M. I.; Serna, C. J. Surface and internal spin canting in γ-Fe_2O_3 nanoparticles. *Chem. Mater.* **1999**, *11*, 3058–3064.

38 Morales, M. P.; Serna, C. J.; Bødker, F.; Mørup, S. Spin canting due to structural disorder in maghemite. *J. Phys.: Condens. Matter* **1997**, *9*, 5461–5467.

39 Choi, J.; Oh, S. J.; Ju, H.; Cheon, J. Massive fabrication of free-standing one-dimensional Co/Pt nanostructures and modulation of ferromagnetism via a programmable barcode layer effect. *Nano Lett.* **2005**, *5*, 2179–2183.

40 Weissleder, R.; Lee, A. S.; Fischman, A. J.; Reimer, P.; Shen, T.; Wilkinson, R.; Callahan, R. J.; Brady, T. J. *Radiology* **1991**, *181*, 245–249.

41 Tanimoto, A.; Kuribayashi, S. *Eur. J. Radiol.* **2006**, *58*, 200–216.

42 Koenig, S. H.; Keller, K. E. Theory of 1/T1 and 1/T2 NMRD profiles of solutions of magnetic nanoparticles. *Magn. Reson. Med.* **1995**, *34*, 227–233.

43 Wille, H.; Drewes, G.; Biernat, J.; Mandelkow, E.; Mandelkow, E. M. Alzheimer-like paired helical filaments and antiparallel dimers formed from microtubule-associated protein tau in vitro. *J. Cell Biol.* **1992**, *118*, 573–584.

44 Winfree, E.; Liu, F. R.; Wenzler, L. A.; Seeman, N. C. Design and self-assembly of two-dimensional DNA crystals. *Nature* **1998**, *394*, 539–544.

45 Lee, H. Y.; Sacho, Y.; Kanki, T.; Tanaka, H.; Shirakawa, H.; Cheon, J.; Yoon, J.-H.; Kang, N.-J.; Park, J.-I.; Kawai, T. DNA-directed magnetic network formation with ferromagnetic nanoparticles. *J. Nanosci. Nanotechnol.* **2002**, *2*, 613–615.

46 Hayes, M. A.; Polson, N. A.; Phayre, A. N.; Garcia, A. A. Flow-based microimmunoassay. *Anal. Chem.* **2001**, *73*, 5896–5902.

47 Pamme, N.; Manz, A. On-chip free-flow magnetophoresis: Continuous flow separation of magnetic particles and agglomerates. *Anal. Chem.* **2004**, *76*, 7250.

48 Fan, Z. H.; Mangru, S.; Granzow, R.; Heaney, P.; Ho, W.; Dong, Q.; Kumar, R. Dynamic DNA hybridization on a chip using paramagnetic beads. *Anal. Chem.* **1999**, *71*, 4851–4859.

49 Hahn, Y. K.; Jin, Z.; Kang, H.; Oh, E.; Han, M.-K.; Kim, H.-S.; Jang, J.-t.; Lee, J.-H.; Cheon, J.; Kim, S.-H.; Park, H. S.; Park, J.-K. Magnetophoretic immunoassay of allergen-specific IgE in an enhanced magnetic field gradient. *Anal. Chem.* **2007**, *79*, 2214.

50 Tizard, I. R. *Immunology*, 4th ed.; Saunders College Publishing: Orlando, FL, 1995.